\$ SUPER

Contents lists available at ScienceDirect

LITHOS

journal homepage: www.elsevier.com/locate/lithos



Continental flood basalts sample oxidized mantle sources

Robert W. Nicklas ^{a,*}, James M.D. Day ^b, Robert B. Trumbull ^c, Haider Rangwalla ^b, Savannah Kelly ^b

- ^a Department of Earth and Environmental Sciences, Boston College, Chestnut Hill, MA 02467, USA
- ^b Scripps Institution of Oceanography, University of California San Diego, La Jolla, CA 92093, USA
- ^c GFZ German Research Centre for Geosciences, Telegrafenberg, 14473 Potsdam, Germany

ARTICLE INFO

Keywords:
Large igneous province
Oxygen fugacity
Olivine

ABSTRACT

Large igneous provinces (LIP) are vast $(0.2 \text{ to } > 1 \text{ Mkm}^3)$ outpourings of basaltic lava and voluminous intrusions of magmas that have had important environmental consequences, in many cases leading to immense greenhouse gas release and mass extinctions. Magmatic oxygen fugacity (fO2) influences the chemistry of volcanic gases and is an important parameter for examining the links between LIP eruptions and environmental change. To constrain the fO2 of LIP magmas, we report olivine elemental chemistry of 399 crystals from a set of fifteen olivine-rich LIP samples, spanning in age from the Proterozoic (~1270 Ma) to the Miocene (~17 Ma). Concentrations of V in olivine are used to show that mafic LIP lavas erupted at $+1.20\pm0.95$ Δ FMQ, on average more oxidized than mid ocean ridge basalts (MORB) at -0.28 ± 0.28 Δ FMQ. Mafic LIP magmas show a much larger range than MORB, however. Additionally, fO2 shows a negative correlation with parental magma MgO content, with high MgO lavas approaching the MORB range. This correlation is likely due to sampling of a heterogeneous mixture of oxidized and reduced lithologies, as also sampled by ocean island basalts (OIB). Correlation between fO2 and isotopic ratios such as 143Nd/144Nd demonstrates that the oxidized endmember is geochemically enriched, and may result from subduction recycling of oxidized surficial materials. The high fO2 of primitive LIP magmas demonstrate that they largely emitted oxidized gases during eruption, and furthermore, that LIP magmas associated with mass extinctions have similar magmatic fO_2 to those that are not. Global plate tectonic position, magnitude and duration of LIP volcanic eruptions and magmatic degassing, as well as interaction with sedimentary basins in the crust - but not mantle source fO_2 - are likely to be the critical factors for whether a LIP was associated with a mass extinction.

1. Introduction

Continental large igneous provinces (LIP), are typically short lived ($<10\,\mathrm{Ma}$, typically $\sim1\,\mathrm{Ma}$) magmatic events that, in some cases, erupted more than one million cubic kilometers of largely homogenous basaltic lavas (e.g., Black et al., 2021; Mahoney and Coffin, 1997; Saunders et al., 1997). It is generally considered that global examples of LIP result from the initial impingement of hot mantle plumes at the base of the continental lithosphere engendering asthenospheric melting. This then leads to large magma volumes, due to their high melting temperatures and lack of association with plate boundaries (Black et al., 2021; Campbell, 2005). Eruptions of LIP occurred from the Archean to the present day, and one has erupted on average every $\sim32\,\mathrm{Ma}$ over the past 250 Ma (Rampino and Stother, 1988). Continental LIP may be not only an important mechanism for cooling Earth's interior but also for solid

earth-atmospheric interactions, due to extensive aerosol and gas release, sometimes resulting in catastrophic mass extinctions (e.g., Wignall, 2001). The most widely accepted LIP to have engendered mass extinction is the Siberian Traps LIP, which is associated with the Permian-Triassic mass extinction, the most extensive such event in Earth history (Burgess et al., 2017; Svensen et al., 2009).

Volcanic gases include both oxidized and reduced species for all major volatile elements (e.g., H_2 and H_2O , CH_4/CO and CO_2 , H_2S and SO_2 ; e.g., Pernet-Fischer et al., 2017). Large-scale LIP volcanic degassing had a variety of environmental consequences, including global cooling by sulphate aerosols, acid rain due to atmospheric SO_2 injection, and global warming due to a spike in atmospheric CH_4 and CO_2 . Although the compositions of volcanic gases are affected by a variety of parameters, such as temperature and pressure during degassing (Kump and Barley, 2007), one of the most important is the oxygen fugacity of the

E-mail address: nicklasr@bc.edu (R.W. Nicklas).

^{*} Corresponding author.

parental magma (Kasting et al., 1993) derived from the oxygen fugacity of the mantle source region (Birner et al., 2018). Oxygen fugacity also has a major effect on the solubility of volatile species in a degassing magma (Jugo et al., 2010) and therefore constraints on the fO_2 of LIP melts are critical for understanding the environmental effects of LIP emplacement and for establishing a link between LIP eruption and mass extinctions (Black et al., 2021). Additionally, LIP are often associated with economically important sulfide ores of Ni and the platinum group elements (e.g., Ernst and Jowitt, 2013; Lightfoot and Keays, 2005). The point of sulfide saturation in a silicate melt is intimately related to magmatic fO_2 (Jugo et al., 2010) and understanding LIP magma fO_2 is therefore critical for modeling LIP-associated sulfide deposit formation. Indeed, it has been previously suggested that oxidized Emeishan LIP lavas gave rise to Fe-Ti oxide deposits, while reduced Emeishan lavas gave rise to sulfide deposits (Cao and Wang, 2022).

To constrain the fO2 of LIP magmas and the relationship between fO2 and mass extinction, we report nearly 400 new olivine trace element analyses for samples from five LIP ranging in age from the Mesoproterozoic to the Miocene (Fig. 1). The concentration of V in olivine can be used to constrain the fO_2 of their parental magmas (Canil, 1997; Humphreys et al., 2022; Nicklas et al., 2022a, 2022b, 2024a, 2024b; Wang et al., 2019). Magmatic fO₂ determined using a similar method has been reported for a wide variety of komatiites, many of them postulated to be associated with Archean LIP (Nicklas et al., 2018, 2019). Samples for this study were chosen for their elevated modal olivine abundances and relatively primitive nature (Fig. S1). They comprise four basaltic lavas from the Upper Steens Formation of the Miocene Columbia River LIP (CRLIP; CR14-03-, CR14-07, CR14-08 and CR14-11), one basaltic lava from the Paleocene Deccan Traps (DC-14-47B), one olivine gabbro sample (Cuillin) and two picrites (SK204, EG2240) from the Paleocene North Atlantic Igneous Province (NAIP), three picritic dikes (KT-10-3, KT-10-5, KT-10-7) and two olivine gabbros (JDNM13, JDNM14) from the Cretaceous Parana-Etendeka LIP, and two picritic lavas from the Proterozoic Copper Creek Formation of the Mackenzie LIP (98-109, 98-119B). The Deccan Traps are associated with a mass extinction event (Wignall, 2001), while the Columbia River LIP, the NAIP, the Parana-Etendeka LIP and the Mackenzie LIP are not. This sample set was used to constrain both the average magmatic fO2 of continental LIP and to examine the potential link between LIP fO2 and environmental change.

2. Methods

Bulk rock geochemical data including major- and trace-element abundances and Rb-Sr, Sm-Nd and Re-Os isotope systematics have been reported previously for most of the studied rocks (Day et al., 2013, 2021; Ellam and Stuart, 2004; Peters et al., 2017; Stroncik et al., 2017). The exceptions are Cuillin, JDNM13 and JDNM14, and for these three samples we determined bulk-rock major and minor element abundances by X-ray fluorescence (XRF: JDNM13, JDNM14, Cuillin) as well as trace element abundances by inductively coupled plasma mass spectrometry for Cuillin, using standardized procedures (Day et al., 2021). Olivine major element data for most samples have been reported previously (Day et al., 2013, 2021; Stroncik et al., 2017; Day, 2016: Peters et al., 2017), while new data are reported here for olivine in the Copper Creek samples. For these analyses, elements of interest were Si, Ti, Al, Cr, Fe, Co, Ni, Mn, Mg and Ca, which were measured using a JEOL 8230 SuperProbe electron probe at the University of Colorado, Boulder using a combination of natural and synthetic mineral standards.

Olivine trace element data were gathered for samples using olivine grain mounts (SK204, EG2240) or commercially prepared polished thin sections (all other samples). Analyses were performed by Laser Ablation ICP-MS (LA-ICP-MS) using a New Wave UP213 (213 nm) laser, coupled to a Thermo Scientific iCAPq Qc ICP-MS at the Scripps Isotope Geochemistry Laboratory (SIGL). Between 7 and 40 spots were analyzed in each sample. Each spot was 100 μm in diameter and each \sim 40 s analysis window was preceded by \sim 20 s of background signal. The laser was operated at 5 Hz with a fluence controlled between 3.0 and 3.5 J/cm². Isotopes of interest were ²⁵Mg, ²⁷Al, ²⁹Si, ⁴³Ca, ⁴⁵Sc, ⁴⁷Ti, ⁵¹V, ⁵⁷Fe, ⁵⁹Co, ⁶⁰Ni, $^{71}\mbox{Ga},\,^{89}\mbox{Y}$ and $^{90}\mbox{Zr}.$ Where available (i.e. Copper Creek samples), data were normalized to average Si abundances determined by electron microprobe. Where Si abundance data were not available, the relatively simple crystal chemistry of olivine was utilized to calculate Si abundance from the average molar Fe/Mg ratio, assuming that olivine only contains significant FeO, MgO and SiO2. These assumptions are unlikely to lead to significant additional uncertainty as Si abundance varies only between 176,200 and 191,551 $\mu g/g$ (8% variation) as olivine forsterite number varies between 70 and 90, which is well below the 2SD variation of V concentration in all the samples (~20%). Standards used in the LA-ICP-MS analyses were USGS reference glasses BHVO-2 g and BCR-2 g, the use of which as standards for olivine has been demonstrated to yield

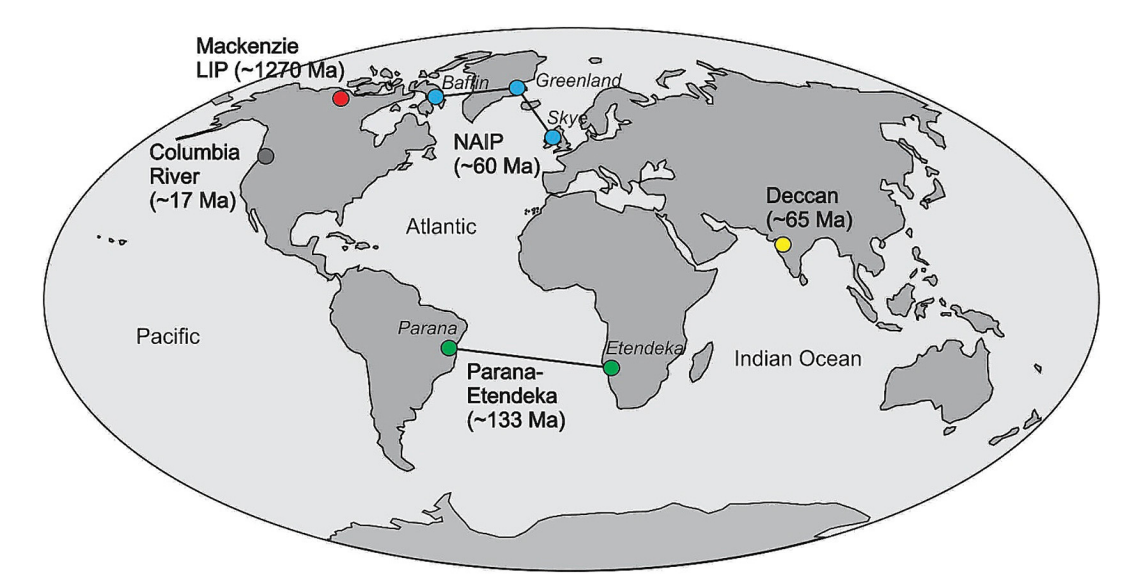


Fig. 1. Map of studied large igneous provinces with approximate maximum emplacement ages.

Ages are taken from Moore et al. (2018) (Columbia River), Hamilton et al. (1998) (NAIP = North Atlantic Igneous Province), Duncan and Pyle (1988) (Deccan = Deccan Traps CFB), Renne et al. (1996) (Parana-Etendeka CFB), and Day et al. (2013) (Mackenzie LIP). Tie lines for the NAIP and Parana-Etendeka LIP denotes dissection of these LIP by opening of the Atlantic Ocean.

accurate V concentration results at the $<5~\mu g/g$ level (Nicklas et al., 2021). Data were reduced using an in-house macro and integration windows were individually examined to exclude any portions of the spectrum that showed evidence of inclusion ablation. The macro considers the limit of detection to be three standard deviations of the background signal for each element. Long-term analyses of an international olivine standard (MongOl) in the same laboratory are plotted with the data in Fig. 1 demonstrating reproducibility of the method.

The partitioning of V into olivine $(D_V^{\text{olivine/melt}})$ has been parameterized as a function of fO_2 , temperature and parental melt composition, most recently by Wang et al. (2019), who incorporated all previously published experimental data. Their empirical equation shows that $D_V^{\text{olivine/melt}}$ is chiefly controlled by fO_2 of the parental magmas due to the much greater compatibility of V^{+3} in olivine relative to V^{+4-+5} . The result of their parameterization is as follows:

$$\label{eq:log10} \textit{log}_{10} \big(D_{V}^{olivine/melt} \big) = \\ -2.30 - 0.258^{^{*}} (\Delta FMQ) \\ + 1871 \big/ T - 0.24 (NBO/T)$$
 (1)

Where ΔFMQ is fO_2 in log units relative to the fayalite-magnetite-quartz buffer, T is temperature in Kelvin, and NBO/T is the ratio of non-bridging oxygen to tetrahedrally bound oxygen in the parental melt. For the purposes of this study, "parental magma" refers to the silicate liquid in equilibrium with the olivine crystals and should not be confused with magmas which are in equilibrium with mantle lithologies, which are often more magnesian. Parental melt compositions were calculated for each sample by first calculating the parental MgO content from the measured olivine Fo and the bulk rock FeO, then subtracting or adding the measured olivine composition from the bulk composition until its MgO content matched that calculated for the parental magma. This method is valid for primitive parental magmas that only crystallized olivine, i.e., those with >7.5 wt% MgO (Nicklas et al., 2024a).

The validity of the oxybarometry method rests upon the measured olivine grains being related to their carrier magmas by crystal-liquid fractionation. This method fails if olivine grains are xenocrysts, i.e. they are unrelated to their bulk rocks. Two lines of evidence indicate that the olivine analyzed here is not xenocrystic: firstly, the low Fo and high Ca contents of the olivine precludes them from being mantle xenocrysts (Table 1), which consistently show lower Ca and higher Fo (i.e. De Hoog et al., 2010). Secondly, while it is possible that xenocrystic olivine can be acquired from an unrelated crystal mush during transit or storage of magmas within the crust (i.e. Thomson and Maclennan, 2013), the olivine populations in this study are unimodal in V contents (Dataset S1), implying that either all or none of the olivine grains sampled are xenocrystic. Given the large number of grains analyzed in each sample we consider it unlikely that all can be of a xenocrystic origin but acknowledge that this scenario cannot be completely disregarded.

Calculated parental magma V concentration was combined with the average olivine V concentration to yield a $D_{\rm V}^{\rm olivine/melt}$ for each sample. Temperature and NBO/T were calculated from the parental magma composition using the methods of Nisbet et al. (1993) and Mills (1993), respectively. Uncertainty on calculated fO_2 is ultimately derived from uncertainties on parental magma V content (10% relative) and the two standard deviation uncertainty on olivine V content, although the uncertainty on olivine V content dominated the propagated uncertainties in all cases. No uncertainty was propagated from temperature estimates, as this source of uncertainty has been shown to be minor (Nicklas et al., 2022a). Similar analyses and calculations have previously been performed for a wide range of OIB and MORB samples and further details of the calculations can be found in Nicklas et al. (2022a, 2022b, 2024a, 2024b).

3. Results

Average olivine trace element compositions for the studied samples are reported in Table 1, and complete data compilations are reported in Dataset S1. Average concentrations of V in olivine range from 5.9 \pm 1.1 (KT-10-7) to 18.0 \pm 3.9 (JDNM14) $\mu g/g$ while the average forsterite number varies from 72 in JDNM13 to 89 in KT-10-7. In general,

Table 1 Average concentrations of major and trace elements ($\mu g/g$) of olivine crystals measured in this study.

Sample	N	Mg	Al	Ca	Sc	Ti	V	Mn	Fe	Co	Ni	Zn	Ga	Y	Fe/Mg
CR14-11	40	223,140	234	1814	10.80	107	9.08		161,386	196	1346		0.25	0.19	0.72
2SD		26,210	71	368	1.72	27	5.09		31,012	32	1303		0.12	0.07	0.13
CR14-03	35	233,040	402	2099	9.72	90.0	10.9		147,183	197	1643		0.38	0.30	0.63
2SD		32,904	401	344	1.84	36.5	3.4		20,136	25	233		0.43	1.06	0.05
CR14-07	26	234,525	307	2065	9.62	89.6	10.9		148,172	199	1648		0.21	0.20	0.63
2SD		34,085	137	283	1.76	38.4	3.5		22,295	27	241		0.30	0.17	0.07
CR14-08	18	159,519	1507	8882	9.07	76.1	7.59		106,556	139	1130		0.39	0.33	0.67
2SD		39,489	862	5339	1.09	14.8	2.26		32,929	39	366		0.44	0.14	0.08
SK204	9	238,803	320	1445			6.51	1395	107,549	173	1750	83.4			0.45
2SD		20,887	99	603			2.37	575	34,556	27	1732	24.4			0.17
EG2240	7	256,920	351	1446			6.79	1460	105,786	167	1825	78.0			0.42
2SD		17,763	319	675			2.34	873	57,655	39	2132	34.2			0.25
Cullin	39	277,348	616	2317	10.5	37.5	7.25		79,472	158	2727		0.24	0.15	0.29
2SD		28,107	282	929	2.4	15.7	1.98		12,212	21	404		0.14	0.05	0.05
98-109	19	205,292	1704	1534	9.67		15.1		169,215	195	1453		0.72	0.65	0.81
2SD		72,996	5769	499	1.21		4.4		75,412	58	137		2.32	0.40	0.14
98-119B	31	206,929	100	1295	8.73		15.1		171,358	194	1378		0.25	0.59	0.83
2SD		15,216	44	401	1.53		4.6		14,090	15	120		0.07	0.25	0.05
JDNM13	32	210,281	217	1621	7.04	257.4	14.9		192,514	200	1843		0.47	1.73	0.92
2SD		28,084	336	361	1.82	101.0	6.1		21,538	23	219		0.44	0.47	0.07
JDNM14	39	212,735	284	2357	8.95	114.4	18.0		188,456	204			0.57	0.40	0.89
2SD		14,694	99	474	1.70	47.2	3.9		30,248	15	386		0.22	0.35	0.16
KT-10-3	21	280,029	805	2246	8.80	53.8	4.99		84,315	156	2787		0.32	0.12	0.30
2SD		28,198	662	573	1.64	15.7	2.22		27,780	38	791		0.18	0.03	0.12
KT-10-5	22	257,095	360	4051	9.57	52.3	5.95		122,708	193	1621		0.21	0.14	0.48
2SD		41,965	313	6968	1.22	20.2	1.72		20,814	23	408		0.08	0.06	0.09
KT-10-7	24	269,825	553	2297	8.49	59.3	5.93		73,973	149	2836		0.26	0.14	0.27
2SD		15,794	155	686	1.79	14.6	1.06		6083	11	220		0.07	0.05	0.02
DC-14-47B	37	250,752	273	2332	8.66	124	7.95		139,052	209	1210		0.22	0.13	0.56
2SD		25,521	59	660	1.73	62	1.79		27,317	28	406		0.06	0.05	0.13

N – number of analysis in the each sample, 2SD – two standard deviations of the dataset, Fe/Mg – ratio is microgram/gram/microgram/gram not molar Fe/Mg. Full LA-ICP-MS datasets are included in the Supplemental Dataset S1.

Etendeka and NAIP olivine grains are considerably more primitive than those of the Deccan, Copper Creek and Columbia River lavas. Comparison of Ni contents and forsterite numbers obtained by LA-ICP-MS and electron probe microanalysis methods for Mackenzie LIP olivine grains overlap entirely (Fig. 2), and full EPMA data for the Mackenzie LIP are reported in *Dataset S2*. Although olivine can be readily diffusively reequilibrated with an evolving magma post-crystallization, diffusion coefficients of Fe and Mg ($\sim 10^{-15}$ m²/s at 1300 °C) and V ($\sim 10^{-14}$ m²/s at 1300 °C) are roughly equivalent (Chakraborty, 2010). This, combined with the Fe-Mg disequilibrium between olivine and bulk rock observed in the samples, showing that olivine crystals are antecrysts and not xenocrysts, indicates that the measured V contents likely reflect those of early-formed olivine. Therefore, the calculated fO_2 values represent those from the last equilibration of olivine and parental melt, likely close to the liquidus.

Calculated parental magma compositions have MgO contents ranging from 6.2 wt% in 98-119B to 17 wt% in KT-10-7 (Table 2). Parental magma compositions are universally mafic, with <52 wt% SiO₂. Although the parental magmas with <7.5 wt% MgO may have fractionated minor clinopyroxene in addition to olivine, fractionation of as much as 30% clinopyroxene causes the calculated fO₂ to vary by only \sim 0.3 log units (Nicklas et al., 2022a), which is less than the uncertainties reported. Samples with calculated parental magma composition <7.5 wt% MgO are hereafter referred to as "Evolved LIP" and only discussed in the context of their relationship to higher MgO ("Primitive LIP") magma compositions. For the primitive samples, parental magma

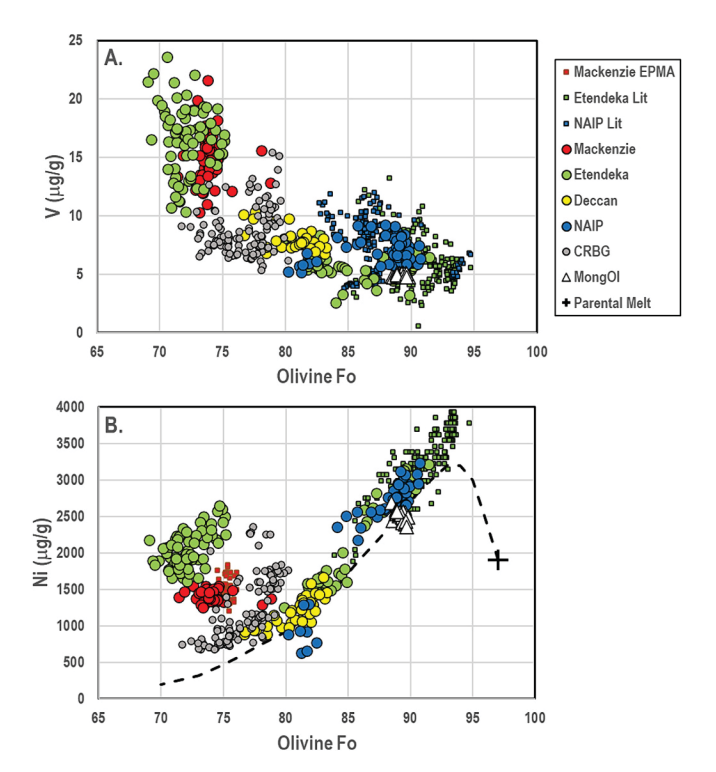


Fig. 2. Concentrations of (a) V and (b) Ni (in $\mu g/g$) in olivine plotted against forsterite number (Fo = $100 \times Mg/(Fe + Mg)$ [in afu]) determined by LA-ICP-MS as larger circles.

Also plotted are electron microprobe (EPMA) data for the same samples of the Mackenzie LIP olivine for Ni, and literature LA-ICP-MS data for the Etendeka and North Atlantic LIP from Cheng et al. (2019) and Nicklas et al. (2019), shown as smaller squares ("EPMA" and "Lit"). Data for the international olivine standard MongOl (Batanova et al., 2019) and the Mackenzie LIP olivine demonstrate reproducibility and close correspondence of Ni using the LA-ICP-MS and EPMA methods. Dotted line in the Ni-Fo figure is from the model after Herzberg (2011) showing the evolution of olivine crystallized from a primary mantle peridotite melt with 28% MgO; primary mantle melts with lower MgO will shift the curve downwards.

 fO_2 shows wide variations ranging from $+0.56^{+0.58}_{-0.43}$ (in Cuillin) to $+2.06^{+0.61}_{-0.45}$ (in KT-10-5) Δ FMQ, with all samples being more oxidized than MORB (Fig. 3). The average of primitive LIP lavas is $+1.2 \pm 1.0$ ΔFMQ, significantly higher than the MORB average using the same oxybarometry method at -0.28 ± 0.28 Δ FMQ (Nicklas et al., 2024a). The fO₂ of the Etendeka dikes reported here overlap with the fO₂ range of +0.4 to $+2.5 \Delta FMQ$ reported for similar Etendeka samples by Cheng et al. (2019). Additionally, the new data plot within the large range of Emeishan LIP lavas of -0.8 to +2.6 Δ FMQ (Cao and Wang, 2022). Considering only the new data, no correlation exists between fO2 and emplacement age (Fig. 4), but a correlation is found when including older komatiite data (Nicklas et al., 2018, 2019). When existing OIB and the new LIP data are combined, fO_2 shows a negative covariation with parental magma MgO content (slope: 0.138 ± 0.044 Fig. 3), a positive covariation with 187 Os/ 188 Os (slope: 15.4 \pm 8.1, Fig. 5a), and a negative covariation with 143 Nd/ 144 Nd (slope: 2679 \pm 1143, Fig. 5b). The MgOfO2 trend is reminiscent of that reported by Wang et al. (2022) for Emeishan LIP high-Ti lavas. Slopes of all three correlations are resolved from zero at 95% confidence intervals. A regression of oxygen fugacity against olivine ${}^{3}\text{He}/{}^{4}\text{He}$ (slope: -0.013 ± 0.023 Fig. 6) for the combined plume lava dataset, however, shows a slope indistinguishable from zero, and no correlation.

4. Discussion

4.1. CFB magmas are oxidized relative to MORB

The studied LIP samples are generally more oxidized than MORB lavas (V-in-olivine oxybarometry = $-0.28 \pm 0.28 \Delta FMQ$; Nicklas et al., 2024a; XANES oxybarometry = +0.1 to -0.2 ± 0.2 Δ FMQ; Berry et al., 2018; Zhang et al., 2018). Parental magmas of some of the studied LIP are notably more evolved (i.e., low MgO) than most previously published OIB samples (Fig. 3). The more evolved nature of the studied LIP lavas versus OIB likely relates to their magmatic plumbing systems within a thicker continental lithosphere that increases the potential for significant fractional crystallization (e.g., Cheng et al., 2019; Day et al., 2021; Peters et al., 2017). The Copper Creek Formation samples of the Mackenzie LIP are picritic in bulk rock composition (Day et al., 2013), but their low olivine Fo (~Fo₇₄), means they may have experienced cofractionation of other phases along with olivine. Despite this, even including the Copper Creek Formation samples, by far the oldest analyzed here, no correlation is observed between emplacement age of LIP and magmatic fO₂ (Fig. 4), consistent with previous conclusions based on komatiites, which showed that mantle-derived magma fO2 stopped changing significantly at ~1.9 Ga (e.g., Nicklas et al., 2019). Notably, the average fO_2 of primitive LIP lavas is $+1.2 \pm 1.0 \Delta FMQ$ (2SD, n = 9), which is identical within uncertainties to the average of all LIP samples at $+1.2 \pm 0.9 \Delta$ FMQ (2SD, n=15).

4.2. Secondary effects on fO2

The fO_2 of mantle-derived magmas reflects the oxidation state of their mantle source regions (Birner et al., 2018; Moussallam et al., 2023; Nicklas et al., 2022a, 2024b) but may also relate to secondary processes such as crustal contamination (Grocke et al., 2016; Nicklas et al., 2022b), degassing of SO_2 (Moussallam et al., 2019), fractional crystallization (Kelley and Cottrell, 2012), and variable partial melting (Gaetani, 2016). Additionally, mixing in of oxidized recycled materials (i.e. Moussallam et al., 2019; Nicklas et al., 2024b) may oxidize the mantle sources of lavas. Each of these processes are considered here in turn to explain the MgO- fO_2 and MgO-isotopic correlations observed in Figs. 3 and 5.

Assimilation of oxidized lithologies within the crust may have increased the fO_2 of LIP magmas, but highly oxidized Fe-rich crustal lithologies are necessary to oxidize mafic lavas while preserving their mafic nature (Nicklas et al., 2022b). Iron-poor crustal lithologies such as

 $\begin{tabular}{ll} \parbox{0.5cm} Table 2 \\ Parental magma compositions of studied layas calculated by olivine subtraction. \\ \parbox{0.5cm} \parbox{0.5cm} Table 3 \\ \parbox{0.5cm} \$

Sample	CK14-11	CR14-03	CR14-07	CR14-08	SK204	EG2240	Cullin	98–109	98-119B	JDNM13	JDNM14	KT-10-3	KT-10-5	KT-10-7	DC-14-47B
Locality	CRB	CRB	CRB	CRB	NAIP	NAIP	NAIP	Mackenzie	Mackenzie	Etendeka	Etendeka	Etendeka	Etendeka	Etendeka	Deccan
SiO_2	48.7	49.1	49.1	48.8	46.5	46.4	48.6	48.0	47.9	43.6	44.3	49.5	50.6	48.3	47.7
TiO_2	2.55	2.17	1.82	1.86	2.79	2.85	0.69	1.18	1.10	2.74	2.57	0.83	1.13	1.08	2.66
Al_2O_3	14.4	16.4	15.6	16.5	8.70	8.9	13.6	14.1	15.6	12.9	12.0	13.9	13.5	11.2	12.0
FeO	13.5	11.7	11.7	11.4	14.0	14.0	10.4	11.0	10.9	15.4	14.9	9.7	10.6	10.9	12.0
MnO	0.22	0.19	0.20	0.15	0.17	0.17	0.18	0.11	0.05	0.22	0.20	0.16	0.18	0.17	0.20
MgO	7.99	6.36	7.93	7.38	14.7	14.2	15.4	6.18	6.15	7.15	7.34	13.2	10.3	17.0	9.61
CaO	8.08	9.01	10.4	10.5	9.87	10.1	10.2	18.3	16.6	14.5	15.2	11.3	11.3	9.42	12.8
Na ₂ O	3.01	3.15	2.66	2.75	1.96	2.00	0.67	0.58	1.21	2.50	2.66	1.22	1.81	1.65	1.86
P_2O_5	0.43	0.58	0.22	0.23	0.35	0.36	0.04	0.11	0.12	0.26	0.19	0.07	0.10	60.0	0.27
K_2O	1.04	1.36	0.40	0.51	0.93	0.95	0.20	0.54	0.35	0.73	0.58	0.18	0.43	0.24	0.88
NBO/T	0.80	99.0	0.77	0.72	1.41	1.39	1.09	0.94	0.84	1.13	1.18	1.00	0.91	1.28	1.05
V (microgram/gram)	367	305	332	304	267	272	241	387	397	009	675	245	349	325	343
Temp (K)	1433	1400	1432	1421	1566	1558	1581	1397	1396	1416	1420	1623	1460	1519	1465
ΔFMQ	1.63	1.81	1.19	1.73	0.65	99.0	0.56	0.87	1.00	1.37	1.20	1.18	2.06	1.41	1.39
Up	1.42	0.53	0.69	0.63	0.80	0.75	0.58	0.62	0.65	0.93	0.46	1.03	0.61	0.38	0.48
Down	0.76	0.4	0.49	0.46	0.54	0.52	0.43	0.42	0.47	0.59	0.36	0.63	0.45	0.31	0.37
XPx	0.55	0.31	0.67	0.34			0.37	0.79	0.74	1.31	1.59	0.41	0.36	0.37	0.25
2SD	0.88	0.34	0.08	0.28			0.12	0.27	0.14	0.23	0.26	0.15	0.10	0.08	0.13
$^3{ m He}/^4{ m He}$					1.10	9.70						19.82	9.45	7.91	10.7
$^{87}\mathrm{Sr}/^{86}\mathrm{Sr}$	0.70342	0.70398	0.70348									0.70690	0.70563	0.70400	
143 Nd 144 Nd	0.51299	0.51283	0.51295									0.51273	0.51263	0.51279	
$^{187}O_{\rm S}/^{188}O_{\rm S}$	0.13056	0.13054	0.13082	0.13132				0.12755	0.12642						0.12260

buffer calculated using Eq. (1) of Wang et al. (2019). Also included are bulk rock Sr-Nd-Os isotope ratios and olivine hosted He isotope ratios, sources of isotopic data are identical to Fig. 5. Up – positive uncertainty on fO₂, X_{px} average olivine Ni enrichment at a given Fo number, after Sobolev et al. (2008), 2SD – two standard deviation uncertainty on average XPx. CRB – Columbia River Basalts, NAIP – All major element oxide concentrations are in wt%, V concentrations are in microgram/gram. NBO/T - non-bonding oxygen to tetrahedrally bonded oxygen ratio calculated from parental magma compositions using the algorithm of Mills (1993). Temp - temperature in kelvin calculated from parental magma MgO content using the equation of Nisbet et al. (1993). AFMQ - calculated fO2 in log units relative to the fayalite-magnetite-quartz North Atlantic Igneous Province.

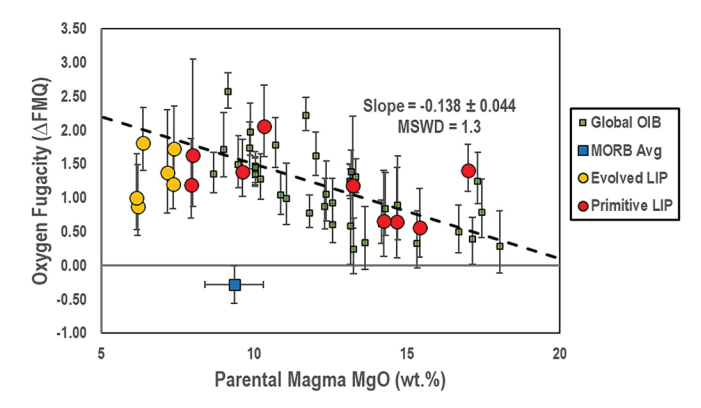


Fig. 3. Calculated fO_2 (in log units FMQ) plotted against parental magma MgO contents (in wt%).

OIB data are from Nicklas et al. (2022a, 2024b) while MORB parental magma composition is from Gale et al., 2013 and the MORB range of fO_2 is from Nicklas et al. (2024a). Dashed line is a linear regression line, excluding the evolved LIP samples. The slope of the regression is listed along with its 95% confidence interval.

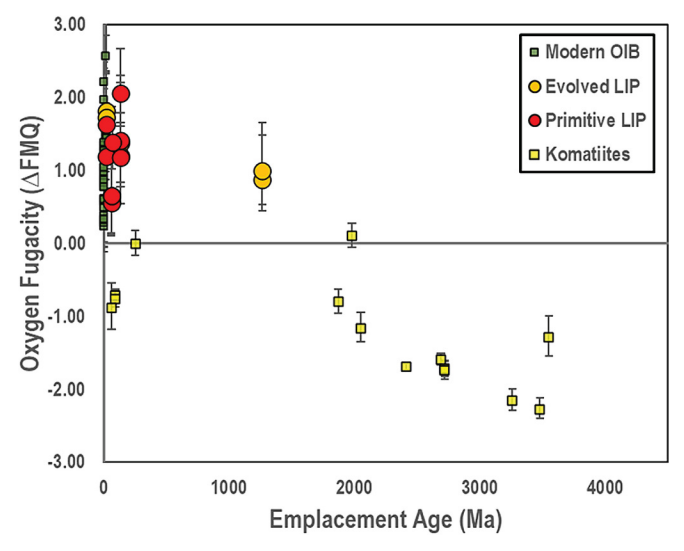
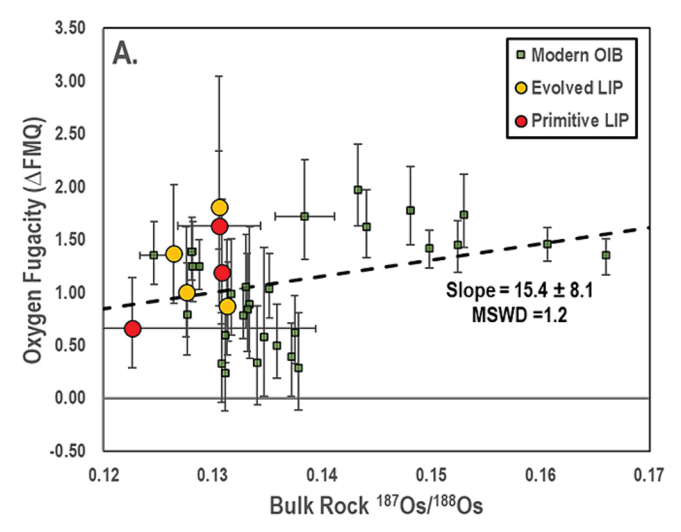


Fig. 4. LIP lava fO_2 plotted versus emplacement age. Also included are OIB data from Nicklas et al. (2022a, 2022b, 2024b), the MORB average from Nicklas et al. (2024a) and komatiite data from Nicklas et al. (2024a). Age data are from Moore et al. (2018) (Columbia River), Hamilton et al. (1998) (North Atlantic), Duncan and Pyle (1988) (Deccan), Renne et al. (1996) (Etendeka), and Day et al. (2013) (Mackenzie).

granites are dominant in the continental crust and are poor oxidizers of basalts (Grocke et al., 2016). If crustal assimilation did occur in the sample set, it left limited imprint (Fig. 5), as isotopic signatures are consistent with relatively limited contamination (Day et al., 2021; Peters et al., 2017; Stroncik et al., 2017). Indeed, even Andean arc basalts with ⁸⁷Sr/⁸⁶Sr ranging up to 0.712 (>30% crustal assimilation) show no resolvable increase in $Fe^{+3}/\Sigma Fe$ (Grocke et al., 2016), indicating that crustal assimilation has limited effect on fO2. Given the significant isotopic variations present in continental crustal materials, oxidation by crustal assimilation cannot be wholly ruled out in general, as each LIP suite may define a unique contamination pathway pointing towards the composition of continental crust local to their region (e.g., Day, 2016). As Fe⁺³/ Σ Fe valence data are not currently available for country rocks near any of the LIP suites examined here, the specific effects of crustal assimilation cannot be quantitatively modeled. However, given that both continental LIP and OIB lavas plot on a single global fO_2 -143Nd/144Nd trend (Fig. 5b), and that even high amounts of crustal



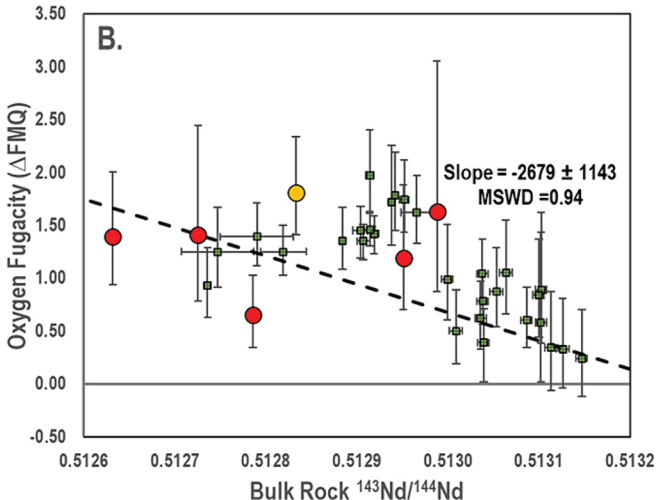


Fig. 5. Calculated fO_2 (in log units FMQ) plotted against bulk rock (a) 187 Os/ 188 Os and (b) 143 Nd/ 144 Nd. Also included are OIB data from Nicklas et al. (2022a, 2024b).

LIP isotopic data are taken from Day et al. (2021) (Columbia River), Peters et al. (2017) (Deccan), Stroncik et al., 2017 (Etendeka), and Day et al. (2013) (Mackenzie). Dashed lines are linear regression of all data except for the evolved LIP samples. Slope of the regression is listed along with its 95% confidence interval.

assimilation in the Andean context has a negligible redox effect (Grocke et al., 2016), we conclude that continental assimilation is unlikely to be the controlling factor of fO_2 in the sample set.

Degassing of SO₂ and fractional crystallization of phases low in ferric iron may have a strongly reducing (Moussallam et al., 2019) or slightly oxidizing (Kelley and Cottrell, 2012) effect on melt fO2, respectively. It has been previously modeled that fractional crystallization of olivine will oxidize magmas by ~ 0.03 log units for every 1 wt% reduction in MgO content (Shorttle et al., 2015). Olivine is the only fractionating phase at low pressure for the primitive magmas (MgO >7.5 wt%) considered here, but the model predicts an oxidation effect of 0.27 log units from the most to least primitive samples in our data set (KT-10-7 to CR14-07), which is within the uncertainties of the oxybarometry method. Additionally, the slope of data for primitive LIP (this study) and OIB (literature) on a plot of MgO and fO2 (Fig. 3) greatly exceeds 0.03 log units/wt%. While SO_2 degassing can strongly affect magma redox conditions, it has only ever been shown to reduce fO2 (Moussallam et al., 2019) and given that degassing occurs as magmas evolve; this process is unlikely to produce a negative correlation of fO2 and MgO. Low degree partial melts can be more oxidized than their mantle source regions due

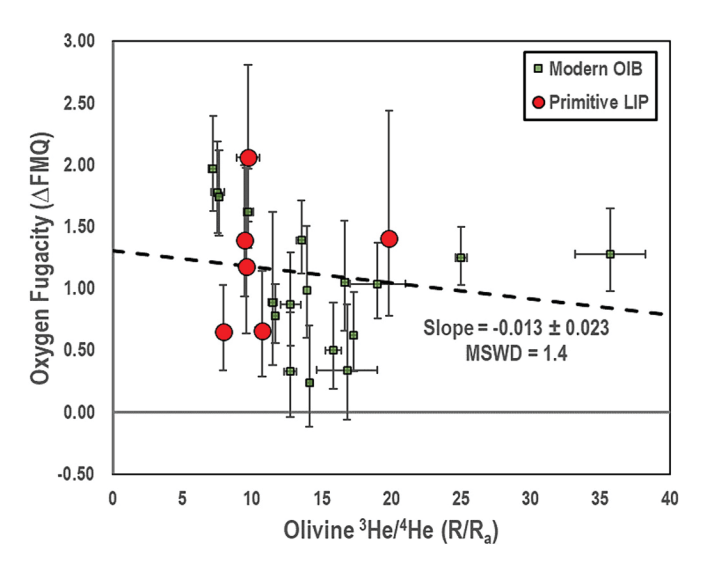


Fig. 6. Calculated fO_2 (in log units FMQ) plotted against $^3\text{He}/^4\text{He}$ of olivine separates.

Also included are OIB data from Nicklas et al. (2022a, 2024b). He isotopic data are taken from Stuart et al. (2000) (NAIP), Day (2016) (NAIP), Peters et al. (2017) (Deccan), and Stroncik et al., 2017 (Etendeka). Dashed line is a linear regression of all the data, the slope is indicated along with its 95% confidence interval.

to the incompatibility of Fe^{+3} relative to Fe^{+2} (Gaetani, 2016), but Nicklas et al. (2024b) showed that the range of fO_2 resulting from 1 to 20% partial melting of homogenous peridotite is insufficient to explain the range of fO_2 shown by the OIB dataset in Fig. 3, and none of the LIP lavas considered here resulted from >20% partial melting. For these reasons, fractional crystallization, degassing, and differential partial melting of a homogenous source can be discounted as the controlling processes on LIP and OIB redox systematics.

4.3. Effects of recycling and metasomatism on mantle sources

It has been posited that some LIP magmas, particularly those from the Etendeka, Deccan and NAIP suites, sample deep mantle reservoirs based on their He isotope systematics (e.g., Marty et al., 1998; Stuart et al., 2000; 2003; Stroncik et al., 2017; Peters et al., 2017). However, the lack of correlation between fO_2 and ${}^3\text{He}/{}^4\text{He}$ in the combined LIP-OIB dataset (Fig. 6) indicates that sampling of a less degassed reservoir appears irrelevant to magma fO2. Similar to what has been previously observed for global OIB lavas, both Nd and Os isotopic signatures correlate with fO₂ in continental LIP (Fig. 3). Indeed, the new data plot on the same correlation trend as the OIB lavas, albeit with considerable uncertainties. The redox systematics of OIB have been suggested to reflect mixing of melts from reduced, refractory mantle lithologies and melts from oxidized, more fusible mantle lithologies that may have resulted from crustal recycling (Nicklas et al., 2024b). Such a scenario has been previously invoked for the oxidized high-Ti lavas and reduced low-Ti lavas of the Emeishan LIP (Wang et al. 2022). Variable melt fractions in the mantle may access different lithologies due to the more fusible nature of recycled, oxidized material (i.e., pyroxenite, metasomatized peridotite) leading to varying proportions of different mantle components in erupted basalts.

It has been postulated that several continental LIP lavas were chiefly sourced from the oxidized, metasomatized sub-lithospheric mantle (i.e., Molzahn et al., 1996; Turner and Hawkesworth, 1995), though it is unclear if such lithospheric metasomes can produce sufficient melt to explain high-volume LIP provinces. However, oceanic lavas like OIB do not pass through ancient, metasomatized lithospheric mantle and therefore cannot sample oxidized lithospheric metasomes. It follows that, since OIB and continental LIP lavas plot on the same fO_2 correlation

trends, an oxidized endmember with a similar fO_2 is necessary; oxidized recycled materials in the asthenosphere are a more logical choice. Subduction of oxidized surficial materials is the simplest way to introduce oxidized and isotopically enriched material into the global asthenosphere, making recycled slab material the most likely oxidized endmember.

4.4. Links between OIB and LIP fO2

Many continental LIP have been shown to predate and be associated with OIB hot-spot tracks, likely as a result of melting in the same hot mantle plume (e.g. Johnson and Thorkelson, 2000). Two plume-LIP associations now have V-in-olivine oxybarometry data published for samples from both OIB and LIP: the NAIP-Iceland plume and the Deccan Traps-Réunion plume associations. Icelandic lavas from Nicklas et al. (2024b) and NAIP lavas overlap entirely with each other, showing a consistent plume source mantle fO_2 with time. La Réunion lavas have been concluded to be crustally contaminated within their edifice (Nicklas et al., 2022b); however, their uncontaminated fO2 likely overlaps with MORB at ${\sim}0~\Delta FMQ$ consistent with XANES estimates (Brounce et al., 2022). It is notable that such low fO2 is also present in low-Ti Emeishan lavas (Wang et al. 2022) indicating that not all plumes incorporate significant oxidized recycled materials. The single Deccan lava analyzed here, DC-14-47B, shows elevated fO_2 at +1.39 Δ FMQ, suggesting that the Reunion plume may have been heterogeneous. Strong conclusions should not be drawn however, given that it was only possible to analyze a single Deccan sample.

4.5. Evaluating pyroxenite melting

The new olivine data were also used to calculate a parameter, X_{Px} , which is a measure of relative Ni enrichment in olivine at a given forsterite number and has been concluded by some (Sobolev et al., 2008) to be a measure of the percentage of pyroxenite melts in a magma. X_{Px} was calculated in the manner of Sobolev et al. (2008) as follows:

$$X_{Px} = (FeO/MgO^*Ni^*0.001341) - 0.437$$
 (2)

Where FeO and MgO concentrations are in wt% and Ni concentration is in $\mu g/g$. X_{Px} was calculated for each individual LA-ICP-MS analysis using measured Fe, Mg and Ni concentrations. The LIP samples show large variations in X_{Px} within a single province (i.e. Etendeka: 0.4 to 1.6), and there is no correlation between average X_{Px} and either isotopic signatures or fO2 (Fig. 7). If only olivine with Fo>80 are considered, all data plot as roughly a single population with $X_{Px} \sim 0.3$ –0.4, while low Fo olivine shows considerable scatter including X_{Px} values >1 and <0. The new data reported here contrast with those of Sobolev et al. (2007) which show X_{Px} clustered around ~ 0.7 for global LIP lavas. Although the average X_{Px} of high Fo olivine could be taken to indicate formation from 30 to 40% pyroxenite melt, this is unlikely given the known effects of varying temperature and pressure on Ni partitioning (Matzen et al., 2017) and the influence of crustal processes which may strongly alter X_{Px} (Gleeson and Gibson, 2019). It is unlikely that three temporally and spatially diverse LIP would be the result of consistently 30-40% pyroxenite melt, instead the high Ni-component may be related to high pressure peridotite melts forming beneath thick continental lithosphere and the roughly consistent X_{Px} across different provinces reflects melting at roughly similar pressures.

4.6. Implications for LIP-induced mass extinction events

The impact of LIP eruptions on the biosphere depends to a significant extent on the amount and type of volcanic gases released. Oxygen fugacity is an important control on the identity of volcanic gases (i.e. Gaillard et al., 2022) in that it affects the balance of oxidized to reduced volatile species (H_2O versus H_2 , CO_2 versus CH_4 and CO_2 versus CO_3 and

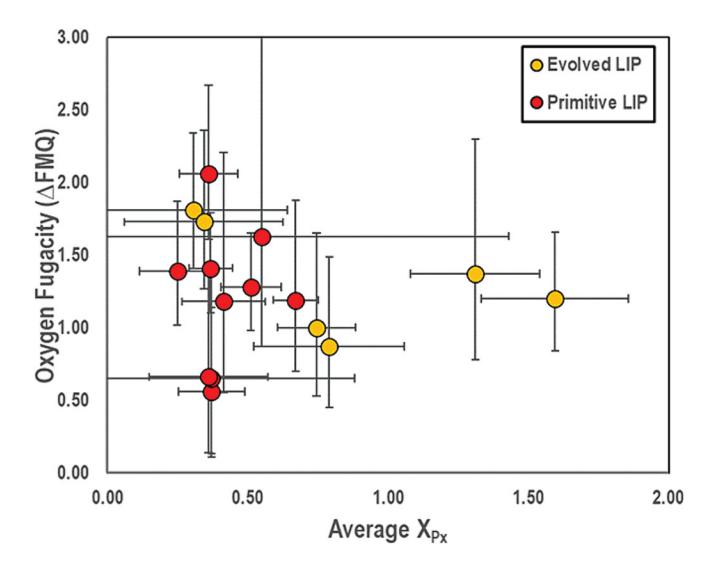


Fig. 7. Calculated fO_2 (in log units FMQ) plotted against the parameter $X_{Px} = (FeO/MgO*Ni*0.001341)-0.437)$ where FeO and MgO are in wt% and Ni is in μ g/g.

 X_{Px} is a measure of Ni enrichment, which possibility indicates pyroxenite melting (Sobolev et al., 2008).

their solubility at specific temperatures and pressures. The oxygen fugacity of a mantle melt closely reflects that of its mantle source region (Birner et al., 2018). As a magma ascends through the crust, fractional crystallization has only a minor effect on magma fO_2 unless magnetite is saturated, which occurs at MgO contents <6 wt% (Kelley and Cottrell, 2012; Shorttle et al., 2015). However, degassing of SO_2 can have a strong reducing effect in a magma due to the necessity of converting dissolved S^{-2} into SO_2 for degassing reducing magmatic Fe^{+3} (Kelley and Cottrell, 2012; Moussallam et al., 2014). Assimilation of strongly oxidized (hematite-rich sediments) or strongly reducing crustal materials (carbonaceous sediments) can alter the fO_2 of an ascending magma (Iacono-Marziano et al., 2012), but this is relatively rare as these materials are typically only available in the uppermost crust. When magma erupts, the temperature, pressure and final fO_2 of degassing all contribute to the ultimate identity of its atmospheric contributions.

Most of the LIP provinces examined here are not known to be associated with any mass extinction (CRB, NAIP, Etendeka and Mackenzie), and only one has been tentatively associated with the end-Cretaceous mass extinction (Deccan; Wignall, 2001). The fO₂ of the single Deccan sample at $+1.39 \Delta FMQ$ plots close to the LIP average. Indeed, the three Etendeka samples range from lower to higher fO2 than the Deccan sample (Table 2). This suggests that pre-contamination magmatic fO_2 is not the determining factor in whether a LIP eruption causes a mass extinction. As has been suggested for the Siberian Traps (Svensen et al., 2009; Burgess et al., 2017; Pernet-Fisher et al., 2017), the influence of crustal assimilation (especially carbonaceous sediments) on volcanic gas chemistry is likely much more important. None of the studied LIP lavas have fO_2 less than $\Delta FMQ \sim 0$, the fO_2 under which reduced volcanic gases such as H2S, CH4, CO and H2 are dominant (Kadoya et al., 2020). Indeed, S⁻² becomes subordinate to S⁺⁶ in natural melts at approximately $fO_2 > +1.9 \Delta FMQ$ in typical mantle-derived magma compositions (Jugo et al., 2010), making significant H2S degassing unlikely. The oxidized nature of LIP lavas indicates that reduced volcanic gases were not dominant during LIP emplacement and that variations in magmatic fO2 cannot explain the lack of mass extinctions associated with specific LIP. The high fO2 of LIP lavas also indicates that any modeling of ore deposit formation must consider the presence of S⁺⁶ in sulfide parental magmas and its effect on sulfur content at sulfide saturation (SCSS).

5. Conclusions

Olivine trace element data are reported for a wide variety of samples from global LIP examples. These data constrain the fO2 of primitive LIP lavas to be $+1.3\pm0.9$ Δ FMQ (2SD). The fO_2 data show no correlation with emplacement age and were not controlled by crustal assimilation, fractional crystallization, or temporal variation in mantle fO2. However, correlations between parental magma MgO, Nd isotopic ratios and fO2 exist, and these correlations are likely related to mixing between oxidized, enriched low-MgO melts and reduced, depleted high-MgO melts, similar to the scenario previously proposed for OIB. The data show that while LIP lavas are generally more oxidized than MORB, high MgO LIP lavas have an fO₂ approaching that of MORB. Such primitive lavas are rarely erupted in continental LIP, and lavas with high fO_2 ($\sim +$ $1~\Delta FMQ)$ likely dominated LIP degassing. The dataset also supports a roughly constant fO2 of plume lavas since the Mesoproterozoic, consistent with previous conclusions based on komatiites (Nicklas et al., 2018, 2019). The parameter X_{Px} is uncorrelated with fO_2 or parental magma composition, indicating that it was likely influenced by crustal processes. High Fo LIP olivine shows consistently $0.3 < X_{Px} < 0.4$ probably as the result of peridotite melting at similar pressures, as opposed to forming from similar proportions of pyroxenite. The LIP samples show insignificant fO2 differences between provinces, and LIP associated with mass extinctions (Deccan) are not more oxidized or reduced than those not associated with mass extinctions (NAIP, Columbia River and Parana-Etendeka). Future atmospheric modeling studies concerning individual mass extinctions and LIP should assume magmatic fO2 from +0.5 to $+2.0 \Delta FMQ$ as opposed to MORB-like values of $\Delta FMQ = 0$. Future studies of more lavas from more LIP provinces will further refine the relationship between eruptive fO₂ and environmental change.

CRediT authorship contribution statement

Robert W. Nicklas: Writing – review & editing, Writing – original draft, Investigation, Formal analysis, Data curation, Conceptualization. James M.D. Day: Writing – review & editing, Funding acquisition. Robert B. Trumbull: Writing – review & editing, Resources. Haider Rangwalla: Formal analysis. Savannah Kelly: Formal analysis.

Declaration of competing interest

The authors declare that they have no known competing financial interests or personal relationships that could have appeared to influence the work reported in this paper.

Acknowledgments

We are grateful to J. Lyakov for development of the in-house LA-ICP-MS data reduction program and L.J. Hulbert for provision of the Coppermine Volcanics samples. This work was funded by National Science Foundation Earth Science Grant #1918322 "A mixed-up mantle beneath Ocean Islands?" to JMDD. This paper benefited from comments by Dr. Wendy Bohrson, an anonymous reviewer, and the co-editor-chief Dr. Greg Shellnut.

Appendix A. Supplementary data

Supplementary data to this article can be found online at https://doi.org/10.1016/j.lithos.2024.107697.

References

Batanova, V.G., Thompson, J.M., Danyusevsky, L.V., Portnyagin, M.V., Garbe-Schonberg, D., Hauri, E., Kimura, J.-I., Chang, Q., Senda, R., Goemann, K., Chauvel, C., Campilo, S., Ionov, D.A., Sobolev, A.V., 2019. New olivine reference material for *in situ* microanalysis. Geostand. Geoanal. Res. 43 (3), 453–473.

Berry, A.J., Stewart, G.A., St. O'Neill, H.C., Mallmann, G., Mosselmans, J.F.W., 2018. A re-assessment of the oxidation state of iron in MORB glasses. Earth Planet. Sci. Lett. 483, 114–123.

- Birner, S.K., Cottrell, E., Warren, J.M., Kelley, K.A., Davis, F.A., 2018. Peridotites and basalts reveal congruence between two independent records of mantle fO_2 despite local redox heterogeneity. Earth Planet. Sci. Lett. 494, 172–189.
- Black, B.A., Karlstrom, L., Mather, T.A., 2021. The life cycle of large igneous provinces. Nat. Rev. Earth Environ. 2, 840–857.
- Brounce, M., Stolper, E., Eiler, J., 2022. The mantle source of basalts from Reunion Island is not more oxidized than the MORB source mantle. Contrib. Mineral. Petrol. 177 (7), 1–18.
- Burgess, S.D., Muirhead, J.D., Bowring, S.A., 2017. Initial pulse of Siberian Traps sills as the trigger of the end-Permian mass extinction. Nat. Commun. 8, 164.
- Campbell, I.H., 2005. Large igneous provinces and the mantle plume hypothesis. Elements 1 (5), 265–269.
- Canil, D., 1997. Vanadium partitioning the oxidation state of Archaean komatiite magmas. Nature 389, 842–845.
- Cao, Y., Wang, C.Y., 2022. Contrasting oxidation state of low-Ti and high-Ti magmas control Ni-Cu sulfide and Fe-Ti oxide mineralization in Emeishan large igneous province. Geosci. Front. 13, 101434.
- Chakraborty, S., 2010. Diffusion coefficients in olivine, wadsleyite and ringwoodite. Rev. Mineral. Petrol. 72, 603–639.
- Cheng, Z., Hou, T., Keiding, J.K., Veksler, I.V., Kamenetsky, V.S., Hornschu, M., Trumbull, R.B., 2019. Comparative geothermometry in high-Mg magma from the Etendeka Province and constraints on their mantle source. J. Petrol. 60 (12), 2509–2528.
- Day, J.M.D., 2016. Evidence against a non-chondritic mantle source for North Atlantic Igneous Province lavas. Chem. Geol. 440, 91–100.
- Day, J.M.D., Pearson, D.G., Hulbert, L.J., 2013. Highly siderophile element behavior during flood basalt genesis and evidence for melts from intrusive chromitite formation in the Mackenzie large igneous province. Lithos 182-183, 242-258.
- Day, J.M.D., Nutt, K.L.R., Mendenhall, B., Peters, B.J., 2021. Temporally variable crustal contributions to primitive mantle-derived Columbia River Basalt Group magmas. Chem. Geol. 572, 120197.
- De Hoog, J.C.M., Gall, L., Cornell, D.H., 2010. Trace-element geochemistry of mantle olivine and application to mantle petrogenesis and geothermobarometry. Chem. Geol. 270, 196–215.
- Duncan, R.A., Pyle, D.G., 1988. Rapid eruption of the Deccan flood basalts at the cretaceous/Tertiary boundary. Nature 333, 841–843.
- Ellam, R.M., Stuart, F.M., 2004. Coherent He-Nd-Sr isotope trends in high ³He/⁴He basalts: implications for a common reservoir, mantle heterogeneity and convection. Earth Planet. Sci. Lett. 228, 511–523.
- Ernst, R.E., Jowitt, S.M., 2013. Large igneous provinces (LIPs) and metallogeny. In:
 Tectonics, Metallogeny, and Discovery: The North American Cordillera and Similar
 Accretionary Settings. Special Publications of the Society of Economic Geologists.
- Gaetani, G.A., 2016. The behavior of Fe³⁺/ΣFe during partial melting of spinel lherzolite. Geochim. Cosmochim. Acta 185, 64–77.
- Gaillard, F., Bernadou, F., Roskosz, M., Bouhifd, M.A., Marrocchi, Y., Iacono-Marziano, G., Moreira, M., Scaillet, B., Rogerie, G., 2022. Redox controls during magma ocean degassing. Earth Planet. Sci. Lett. 577, 117255.
- Gleeson, M.L.M., Gibson, S.A., 2019. Crustal controls on apparent mantle pyroxenite signals in ocean-island basalts. Geology 47 (4), 321–324.
- Grocke, S.B., Cottrell, E., de Silva, S., Kelley, K.A., 2016. The role of crustal and eruptive processes versus source variations in controlling the oxidation state of iron in Central Andean magmas. Earth Planet. Sci. Lett. 440, 92–104.
- Hamilton, M.A., Pearrson, D.G., Thompson, R.N., Kelley, S.P., Emeleus, C.H., 1998.
 Rapid eruption of Skye lavas inferred from precise U-Pb and Ar-Ar dating of the Rum and Cuillin plutonic complexes. Nature 394, 260–263.
- Herzberg, C., 2011. Identification of source lithology in the Hawaiian and Canary Islands: Implications for origins. J. Petrol. 52 (1), 113–146.
- Humphreys, J., Brounce, M., Walowski, K., 2022. Diffusive equilibration of H₂O and oxygen fugacity in natural olivine-hosted melt inclusions. Earth Planet. Sci. Lett. 584, 117409.
- Iacono-Marziano, G., Gaillard, F., Scaillet, B., Polozov, A.G., Marecal, V., Pirre, M., Arndt, N.T., 2012. Extremely reducing conditions reached during basaltic instrusion in organic matter-bearing sediments. Earth Planet. Sci. Lett. 357-358, 319–326.
- Johnson, S.T., Thorkelson, D.J., 2000. Continental flood basalts: episodic magmatism above long-lived hotspots. Earth Planet. Sci. Lett. 175, 247–256.
- Jugo, P.J., Wilke, M., Botcharnikov, R.E., 2010. Sulfur K-edge XANES analysis of natural and synthetic basaltic glasses: Implications for S speciation and S content as function of oxygen fugacity. Geochim. Cosmochim. Acta 74, 5926–5938.
- Kadoya, S., Catling, D.C., Nicklas, R.W., Puchtel, I.S., Anbar, A.D., 2020. Mantle data imply a decline of oxidizable volcanic gases could have trigged the Great Oxidation Event. Nat. Commun. 11, 2774.
- Kasting, J.F., Eggler, D.H., Raeburn, S.P., 1993. Mantle redox evolution and the oxidation state of the Archean atmosphere. J. Geol. 101 (2), 245–257.
- Kelley, K.A., Cottrell, E., 2012. The influence of magmatic differentiation on the oxidation state of Fe in a basaltic arc magma. Earth Planet. Sci. Lett. 329-330, 109-121.
- Kump, L.R., Barley, M.E., 2007. Increased subaerial volcanism and the rise of atmospheric oxygen 2.5 billion years ago. Nature 448, 1033–1036.
- Lightfoot, P.C., Keays, R.R., 2005. Sideropile and chalcophile metal variations in flood basalts from the Siberian Trap, Noril'sk Region: Implications for the origin of the Ni-Cu-PGE sulfide-ores. Econ. Geol. 100, 439–462.
- Mahoney, J.J., Coffin, M.F., 1997. Large igneous provinces: continental, oceanic and planetary flood volcanism. AGU Geophys. Ser. 100 (ISBN: 0-87590-082-8).

Marty, B., Upton, B., Ellam, R., 1998. Helium isotopes in early Tertiary basalts, Northeast Greenland: evidence for 58 Ma plume activity on the North Atlantic-Iceland volcanic province. Geology 26, 407–410.

- Matzen, A.K., Wood, B.J., Baker, M.B., Stolper, E.M., 2017. The roles of pyroxenite and peridotite in the mantle sources of oceanic basalts. Nat. Geosci. 10, 530–535.
- Mills, K.C., 1993. The influence of structure on the physico-chemical properties of slags. ISIJ Int. 33 (1), 148–155.
- Molzahn, M., Reisberg, L., Worner, G., 1996. Os, Sr, Nd, Pb, O isotope and trace element data from the Ferrar flood basalts, Antarctica: evidence for an enriched subcontinental lithospheric source. Earth Planet. Sci. Lett. 144, 529–546.
- Moore, N.E., Grunder, A.L., Bohrson, W.A., 2018. The three-stage petrochemical evolution of the Steens Basalt (Southeast Oregon, USA) compared to large igneous provinces and layered mafic intrusions. Geosphere 14 (6), 2505–2532.
- Moussallam, Y., Oppenheimemr, C., Scaillet, B., Gaillard, F., Kyle, P., Peters, N., Hartley, M., Berlo, K., Donovan, A., 2014. Tracking the changing oxidation state of Erebus magmas, from mantle to surface driven by magma ascent and degassing. Earth Planet. Sci. Lett. 393, 200–209.
- Moussallam, Y., Longpre, M.-A., McCammon, C., Gomez-Ulla, A., Rose-Koga, E.F., Scaillet, B., Peters, N., Gennaro, E., Paris, R., Oppenheimer, C., 2019. Mantle plumes are oxidized. Earth Planet. Sci. Lett. 527, 115798.
- Moussallam, Y., Georgeais, G., Rose-Koga, E.F., Koga, K.T., Hartley, M.E., Scaillet, B., Oppenheimer, C., Peters, N., 2023. CO₂-undersaturated melt inclusions from the South West Indian Ridge record surprisingly uniform redox conditions. Geochem. Geophys. Geosyst. 24 (12) (e2023GC0011235).
- Nicklas, R.W., Puchtel, I.S., Ash, R.D., 2018. Redox State of the Archean Mantle: evidence from V partitioning in 3.5-2.4 Ga Komatiites. Geochim. Cosmochim. Acta 222, 447–466
- Nicklas, R.W., Puchtel, I.S., Ash, R.D., Piccoli, P.M., Hanski, E., Nisbet, E.G., Waterton, P., Pearson, D.G., Anbar, A.D., 2019. Secular mantle oxidation across the Archean-Proterozoic boundary: evidence from V partitioning in Komatiites and Picrites. Geochim. Cosmochim. Acta 250, 49–75.
- Nicklas, R.W., Day, J.M.D., Vaci, Z., Udry, A., Liu, Y., Tait, K.T., 2021. Uniform oxygen fugacity of shergottite mantle sources and an oxidized martian lithosphere. Earth Planet. Sci. Lett. 564, 116876.
- Nicklas, R.W., Hahn, R.K.M., Willhite, L.N., Jackson, M.G., Zanon, V., Arevalo Jr., R., Day, J.M.D., 2022a. Oxidized mantle sources of HIMU- and EM-type Ocean island basalts. Chem. Geol. 602, 120901.
- Nicklas, R.W., Hahn, R.K.M., Day, J.M.D., 2022b. Oxidation of La Reunion lavas with MORB-like fO₂ by assimilation. Geochem. Perspect. Lett. 20, 32–36.
- Nicklas, R.W., Puchtel, I.S., Baxter, E.F., 2024a. Concordance of V-in-olivine and Fe-XANES oxybarometry methods in mid-ocean ridge basalts. Earth Planet. Sci. Lett. 625, 118492.
- Nicklas, R.W., Baxter, E.F., Brandon, A.D., Lonero, A.J., Day, J.M.D., 2024b. Mantle plumes sample heterogeneous mixture of oxidized and reduced lithologies. Chem. Geol. 645, 121897.
- Nisbet, E.G., Cheadle, M.J., Arndt, N.T., Bickle, M.J., 1993. Constraining the potential temperature of the Archean mantle: A review of the evidence from komatiites. Lithos 30, 291–307.
- Pernet-Fischer, J.F., Day, J.M.D., Howarth, G.H., Ryabov, V.V., Taylor, L.A., 2017. Atmospheric outgassing and native-iron formation during carbonaceous sediment-basalt melt interactions. Earth Planet. Sci. Lett. 460, 201–212.
- Peters, B.J., Day, J.M.D., Greenwood, R.C., Hilton, D.R., Gibson, J., Franchi, I.A., 2017. Helium-oxygen-osmium isotopic and elemental constraints on the mantle sources of the Deccan Traps. Earth Planet. Sci. Lett. 478, 245–257.
- Rampino, M.R., Stother, R.B., 1988. Flood basalt volcanism during the past 250 million years. Science 241 (4866), 663–668.
- Renne, P.R., Glen, J.M., Milner, S.C., Duncan, A.R., 1996. Age of Etendeka flood volcanism and associated intrusions in southwestern Africa. Geology 24, 659–662.
- Saunders, A.D., Fitton, J.G., Kerr, A.C., Norry, M.J., Kent, R.W., 1997. The North Atlantic igneous province. In: Mahoney, J.J., Coffin, M.F. (Eds.), Large Igneous Provinces: Continental, Oceanic and Planetary Flood Volcanism. Geophysical Monograph, American Geophysical Union, 100, pp. 45–93.
- Shorttle, O., Moussallam, Y., Hartley, M.E., Maclennan, J., Edmonds, M., Murton, B.J., 2015. Fe-XANES analyses of Reykjanes Ridge basalts: Implications for oceanic crust's role in the solid Earth oxygen cycle. Earth Planet. Sci. Lett. 427, 272–285.
- Sobolev, A.V., Hofmann, A.W., Brugmann, G., Batanova, V.G., Kuzmin, D.V., 2008. A quantitative link between recycling and osmium isotopes. Science 321 (5888), 536
- Stroncik, N.A., Trumbull, R.B., Krienitz, M.-S., Niedermann, S., Romer, R.L., Harris, C., Day, J.M.D., 2017. Helium isotope evidence for a deep-seated mantle plume involved in South Atlantic breakup. Geology 45 (9), 827–830.
- Stuart, F.M., Ellam, R.M., Harrop, P.J., Fitton, J.G., Bell, B.R., 2000. Constraints on mantle plumes from the helium isotopic composition of basalts from the British Tertiary Igneous Province. Earth Planet. Sci. Lett. 177, 273–285.
- Stuart, F., Lass-Evans, S., Godfrey Fitton, J., Ellam, R., 2003. High ³He/⁴He ratios in picritic basalts from Baffin Island and the role of a mixed reservoir in mantle plumes. Nature 424, 57–59. https://doi.org/10.1038/nature01711.
- Svensen, H., Planke, S., Polozov, A.G., Schmidbauer, N., Corfu, F., Podladchikov, Y.Y., Jamtveit, B., 2009. Siberian gas venting and the end-Permian environmental crisis. Earth Planet. Sci. Lett. 277, 490–500.
- Thomson, A., Maclennan, J., 2013. The distribution of olivine compositions in Icelandic basalts and picrites. J. Petrol. 54 (4), 745–768.
- Turner, S., Hawkesworth, C., 1995. The nature of the sub-continental mantle: constraints from the major-element composition of continental flood basalts. Chem. Geol. 120, 295–314.

- Wang, J., Xiong, X., Takahashi, E., Zhang, L., Li, L., Liu, X., 2019. Oxidation state of arc mantle revealed by partitioning of V, Sc and Ti between mantle minerals and basaltic melts. J. Geophys. Res. Solid Earth 124, 4617–4638.
 Wignall, P.B., 2001. Large igneous provinces and mass extinctions. Earth Sci. Rev. 53, 1218
- 1–33.

Zhang, H.L., Cottrell, E., Solheid, P.A., Kelley, K.A., Hirschmann, M.M., 2018. Determination of $Fe^{+3}/\Sigma Fe$ of XANES basaltic glass standards by Mossbauer spectroscopy and its application to the oxidation state of iron in MORB. Chem. Geol.